

Experimental Investigation of Bistable Winglets to Enhance Wing Lift Takeoff Capability

A. Gatto*

Brunel University, Uxbridge, Middlesex, England, UB8 3PH, United Kingdom
and

F. Mattioni† and M. I. Friswell‡

University of Bristol, Bristol, England, BS8 1TR, United Kingdom

DOI: 10.2514/1.39614

An experimental investigation into the use of a bistable winglet to enhance the lift characteristics of a wing transitioning from lower to higher subsonic flow speeds is presented in this paper. The concept centers around the use of a specifically designed composite winglet, manufactured with an unsymmetric layup, which, when increasingly loaded, snaps between two stable states. Initially, during low-speed operation, the winglet is fixed in one stable state that is specifically designed to be cambered, thus enhancing the lift capability of the wing. At higher dynamic pressures, the winglet snaps to a configuration more intuitive and conventional to current winglet design. Results presented in this paper show the concept to be viable at enhancing the lift produced by a swept wing as aerodynamic loading increases before snap-through. During snap-through, however, the absence of any method of controlling the snap-through process generated significant dynamic loading that was transmitted, unhindered, throughout the entire test rig.

Nomenclature

b	=	wing span, m
C_D	=	drag coefficient
C_L	=	lift coefficient
C_Y	=	side force coefficient
C_l	=	rolling moment coefficient
C_m	=	pitching moment coefficient
C_n	=	yawing moment coefficient
$c_{\text{root}}, c_{\text{tip}}$	=	root and tip chords, m
h	=	winglet height
S	=	wing area, m ²
V	=	freestream velocity, m · s ⁻¹
α	=	angle of attack, deg
γ	=	cant angle, measured as dihedral angle relative to wing plane, deg
Λ	=	sweep angle, deg

Subscripts

bs	=	before snap
max	=	maximum
min	=	minimum
rms	=	root mean square
tip	=	tip spanwise location
wl	=	winglet

I. Introduction

A CONCERTED effort currently exists in the aerospace community to develop morphing aircraft systems and technologies [1–7]. Morphing may be broadly defined as the real-

time in-flight adaptability of aircraft systems to optimize and configure themselves to achieve maximum efficiency over a wide range of flight regimes. The primary impetus for this effort is the increased cost-effectiveness that one platform brings to various theaters of operation: high-speed dash for ground and air attack, loiter for surveillance and reconnaissance, or high-lift for takeoff and landing. With these desired but demanding characteristics for morphing aircraft and the use of composite materials firmly embedded in modern aircraft structural design, it is of no great surprise that increasing trends toward developing synergetic symbiotic applications of these two technologies currently exist. This combination of adaptability with high strength/weight aircraft structures, if successful, clearly presents significant advancements for future aircraft configurations.

Unfortunately, however, the use of composite materials within the broad application of morphing technologies presents significant challenges to the aircraft designer and engineer. Although applications do exist [4,8,9], various problems ranging from acceptable methods of actuation [5] and/or power consumption [8,9], achievable and reliable control [10], and substandard performance when compared with existing methods and/or tailorable structural stiffness/compliance [11,12] can be just some examples of limiting factors. Another important aspect of integrating these technologies in morphing aircraft is that morphing aircraft dynamically change state in flight. This particular characteristic does infer a degree of structural compliance, which can also introduce significant secondary aeroelastic challenges such as wing flutter.

One critical phase of flight for any aircraft, morphing or otherwise, is the initial takeoff configuration (principally considered in this paper). In this state, the aircraft weight can be near its maximum, often requiring, particularly for large commercial aircraft, a runway of substantial length to take off safely [13]. For this particular category of modern aircraft, assistance in this phase of the flight envelope is generally provided through the use of deployable slats and flaps that temporarily increase the camber of the wing, thereby generating substantial lift augmentation when compared with normal cruising conditions [14–17]. Unfortunately, however, systems such as these are intrinsically bulky and, due to the need for complex arrangements [18] and/or multiple redundancies, particularly heavy. In fact, the inclusion of one of these systems into a commercial aircraft can add up to 6–10% to the overall wing weight alone [19]. It is for primarily these reasons that alternative methods for generating

Received 9 July 2008; accepted for publication 16 December 2008. Copyright © 2008 by A. Gatto. Published by the American Institute of Aeronautics and Astronautics, Inc., with permission. Copies of this paper may be made for personal or internal use, on condition that the copier pay the \$10.00 per-copy fee to the Copyright Clearance Center, Inc., 222 Rosewood Drive, Danvers, MA 01923; include the code 0021-8669/09 \$10.00 in correspondence with the CCC.

*Lecturer in Aerospace Engineering, Department of Mechanical Engineering, Member AIAA.

†Marie Curie Research Assistant, Department of Aerospace Engineering.

‡Sir George White Professor, Department of Aerospace Engineering.

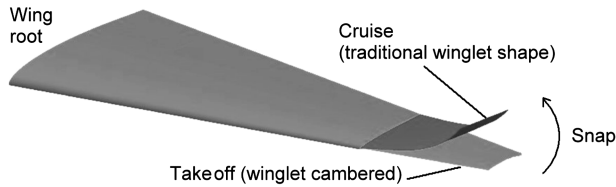


Fig. 1 The bistable winglet concept.

this lift augmentation capability are eagerly sought by aircraft designers and manufacturers.

In this paper, the authors present a concept (Fig. 1) that seeks to merge the two areas of composite materials and morphing aircraft. The concept involves the use of a bistable winglet for lift augmentation at low flight speeds (before takeoff), which has the ability to change to another, more intuitive, winglet configuration [20] at higher flight speeds (climb/cruise). In the transitional region, the winglet is designed to snap, passively, from the first stable state to the second using only the increased aerodynamic loading on the winglet as the dynamic pressure, and/or angle of attack, increases. Among the results presented are the real-time responses of the swept wing and composite winglet to aerodynamic loading before, during, and after the snap process. Overall, these results show the concept's viability and present a firm foundation for future consideration and development.

II. Design and Analysis of Selected Composite Winglet Configurations

Fundamentally, bistable composites are manufactured through the introduction of a residual stress field into the internal structure of the layup by two main mechanisms: prestressing the layup [21] or introducing thermal stresses during manufacture [22]. In this paper, the latter method is employed using an unsymmetric orthotropic-lamina layup sequence. As a result of the unsymmetrical layup sequence and the laminas oriented either 0 or 90 deg, the dissimilar coefficients of thermal expansion about the laminas' principal directions set up the internal structural stresses required for bistability during the cooldown phase of composite manufacture. Ultimately, the resultant laminate obtains multiple dissimilar stable states, each having nonzero out-of-plane displacement.

Another characteristic of thermally induced bistable structures is that the stable states set up from the manufacturing process can be engineered to be flexible and/or stiff, depending on the application. This is principally achieved through the careful and combined selection of material properties, layup sequence, and structural geometry. Furthermore, bistable structures engineered in this way can retain bistability even when constrained under certain conditions (restraining one edge, for example), giving a substantial scope of engineering application. However, perhaps the most distinct advantage of using bistable composites, when compared with other smart structures, is that the required load to effect change is only required momentarily to initiate the transition (no continuous power drain).

The chosen planform for the desired winglet used in all subsequent analysis and wind-tunnel testing is shown in Fig. 2 ($b_{wl} = 0.3$ m,

$c_{root,wl} = 0.185$ m, $c_{tip,wl} = 0.105$ m, and $\Lambda_{wl} = 30$ deg). Ultimately, this planform was selected to ensure seamless compatibility with the baseline swept-wing planform used and described in Sec. III. As shown, the winglet was designed to have two separate sections: the first with bistability and the second without. The second symmetric section was integrated into the winglet to allow ease of transition into the baseline swept-wing-tip assembly. For the initial numerical analysis, the three configurations shown in Fig. 2 were considered before ultimately selecting and manufacturing the best winglet configuration for use with the wind-tunnel model. The first configuration used fibers oriented parallel and perpendicular to the winglet leading edge (LE), with the second incorporating fibers oriented parallel and perpendicular to a line bisecting the midpoints of the root and tip chord. The last, and final, configuration used fibers oriented parallel and perpendicular to a line intersecting the symmetric and unsymmetric layup sections (Fig. 2c). To quantify the resulting shapes of these three configurations and predict subsequent behavior, a nonlinear finite element package (ABAQUS) was used to model standard T300 carbon fiber prepreg, with Hexcel epoxy resin 914 (properties in Table 1) selected as the default material.

For the numerical analysis, a two-stage multistep nonlinear analysis using standard built-in functions within ABAQUS was applied to all of the configurations shown in Fig. 2. For each of these cases, the winglet panel was modeled using 336 double-curvature shell elements (S8R) with a total of 1089 nodes. For the first stage of the analysis, the cooldown process of the laminate during manufacture was simulated, giving the predicted final geometric shapes. For this cooldown stage of the manufacturing process, the simulation procedure involved applying a temperature difference of 170°C (from nominal room temperature) with a heat-up rate of 2–5°C/min to all nodes of the model. During this part of the simulation, the plate was clamped at a point coincident with the origin of the reference system ($X = 0$ and $Y = 0$ in Fig. 3) and at two additional nodes at the midpoint of the root and the tip chords, which were also restrained to move in the X – Y plane. These two additional constraints were only applied temporarily to aid in the convergence of the numerical procedure to a stable solution. At the end of this step, the temperature field was allowed to dissipate naturally back to room temperature. To simulate the mechanics of the snap-through, a concentrated force acting vertically up at the midpoint of the tip chord was applied to the cured composite. For this second stage of the analysis, all nodes at the root section were rigidly clamped, representing boundary conditions indicative of proposed wind-tunnel testing (Fig. 4). A vertical force was then applied at the midpoint of the tip chord, and to eliminate numerical inconsistencies, the same node was also constrained temporarily to move vertically. Before removal of this constraint, the concentrated load was ramped linearly from 0 to 40 N to induce the snap-through, thereafter being removed to ensure convergence to a stable final result. Further information on the numerical procedure employed and an evaluation of this procedure using experimental results can be found in [23].

The first step taken in the numerical design of the winglet was to decide the number of lamina layers to use in the layup with the winglet planform dimensions outlined. For this operation, the configuration shown in Fig. 2b was used. Layups comprising 2, 4, 8, and 12 laminas were investigated. For the 2- and 4-lamina layups, initial analysis showed that the out-of-plane displacements in both

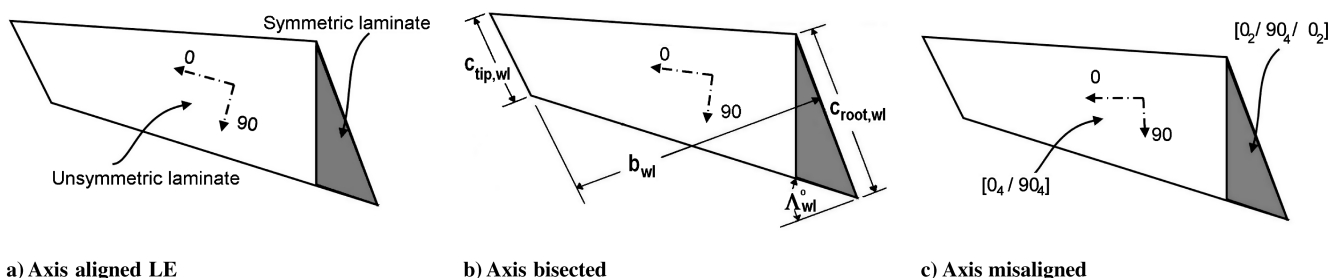


Fig. 2 Composite winglet layup directions investigated.

Table 1 Summary of lamina properties used for layup

Properties	Material	E_{11} , GPa	E_{22} , GPa	G_{12} , GPa	ν_{12}	α_1 , $1/^\circ\text{C}$	α_2 , $1/^\circ\text{C}$	t , mm
Values	T300/914	130	10	4.4	0.33	-0.18×10^{-6}	30×10^{-6}	0.125

stable states were extreme and not suitable for use in the intended application. Using 12 layers resulted in a laminate that was too stiff, with cured curvatures that were inadequate to produce any noticeable effect on the aerodynamics. The only number of layers in the layup giving a reasonable degree of out-of-plane displacement comparable with generic winglet cant-angle geometries for the snapped configuration and possessing sufficient camber in its presnapped state to generate extra lift (without significant separation) was through using eight layers. This number of lamina was therefore fixed for all subsequent analysis.

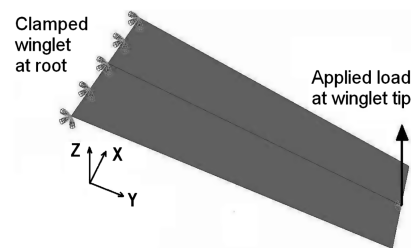
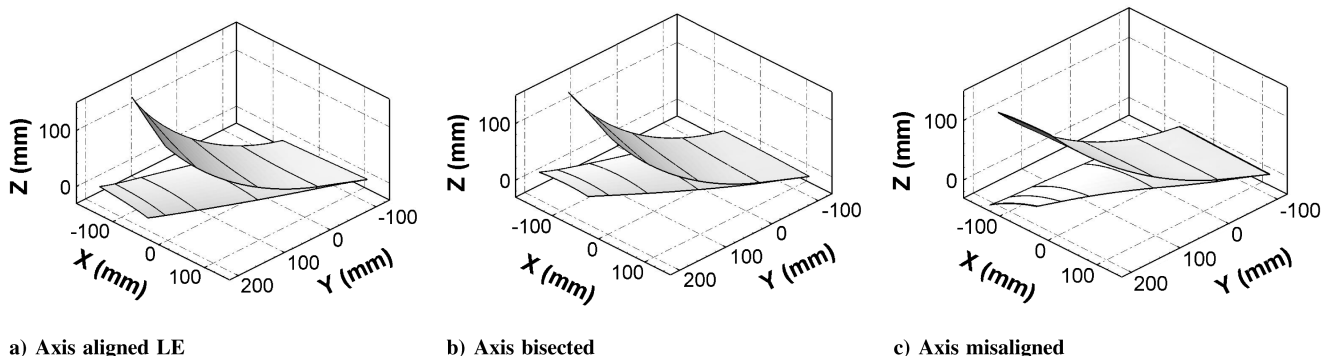
Regarding the general shape of the winglet, it was decided that the final stable states of the bistable composite winglet should possess attributes that meet several different criterion. First, in the unsnapped configuration, the induced chordwise curvature along the span of the winglet should be sufficient enough to produce a measurable enhancement of the lift generated from the test rig. Ideally, this performance increment would match or exceed that achieved by current high-lift systems. In setting this constraint, however, it was realized that due consideration should be given to avoiding severe levels of flow separation. Second, the magnitude of the snap load between the two stable configurations needs to be achievable and within the capabilities of the experimental apparatus used. This was the purpose of the second simulation stage discussed earlier. Finally, in the snapped configuration, the winglet geometry should resemble a traditional winglet design configuration, allowing for the possible exploitation of benefits that such an aerodynamic device can provide [24,25].

With due consideration to these desired constraints, the numerically predicted geometrical shapes obtained from an analysis of the three different configurations was assessed. For case a in Figs. 3a and 5a, results predicted general geometric shapes that were considered to be unsuitable for the proposed application. First, in the unsnapped configuration, there was a tendency for this layup case to exhibit a winglet-tip angle of attack and twist that was inherently negative ($\alpha_{\text{tip}} \approx -6^\circ$), together with no measurable camber (side view in Fig. 5a). The unsuitability of this configuration was further supported by results shown for the rear view in Fig. 5a for the snapped winglet state in which substantial degrees of the LE-down twist at the tip ($\alpha_{\text{tip}} \approx 21^\circ$) are predicted. Ultimately, this combination would promote both decreased sectional lift and increased outboard sectional side force that was dependent on the local cant angle ($\gamma_{\text{max}} = 55.8^\circ$ at the tip).

For the third winglet configuration investigated (Figs. 3c and 5c), the resultant geometric configuration was found to be in direct contrast to that discussed for Figs. 3a and 5a. Under these conditions, the simulated unsnapped configuration was found to exhibit a large degree of winglet twist ($\alpha_{\text{tip}} > 22^\circ$), conducive to the generation of substantial levels of extra lift. Considering the winglet as a thin

airfoil, however, this result clearly suggests the development of sizable portions of flow separation acting at these local angles of attack at these outboard locations [26]. This situation was found to remain unchanged at winglet midspan with the local sectional angle of attack being 10.2° deg, approximately the level at which severe stall conditions are well established on most thin airfoils ($10\text{--}12^\circ$) [26]. These levels of winglet twist and resulting sectional angles of attack were particularly unfortunate for this configuration, as analysis for the snapped configuration (rear view the Fig. 5c) revealed the predicted geometry to possess a moderate, $\alpha = 1.2^\circ$ deg, LE-down wing twist. This value is significantly lower than that found for case a and agrees relatively well with classical winglet design recommendations of 4° deg LE out [27].

For the final case, case b, the predicted geometry was found to lie within the two extremes already considered. In the unsnapped configuration, the winglet was found to exhibit moderate camber values of 3.2 and 6.1% at the tip and midspan of the winglet, respectively. These results were encouraging, establishing the possibility for lift augmentation with low levels of flow separation [26]. Additionally, from analysis of the winglet-tip twist distribution in the unsnapped configuration, overall winglet twist was found to be almost zero along the entire winglet span. This was not, unfortunately, characteristic for the snapped case, with wing twist at the winglet midspan and tip being $\alpha = 10.2^\circ$ deg and $\alpha_{\text{tip}} = 15.7^\circ$ deg, respectively. Additionally, for this deployed configuration, the magnitude of the predicted cant angle was also found to be 53.1° deg, compared with 55.8 and 45.3° deg for cases a and c, respectively. Even at this improved level, 53.1° deg remained significantly lower than that recommended by the classical Whitcomb [27] design specifications ($\gamma = 75^\circ$ deg), but within more modern winglet design philosophies ($45 \leq \gamma \leq 75^\circ$) [28]. This substandard agreement with classical winglet design continued with consideration of the maximum deployed winglet height, with guidelines recommending parity to the wing-tip chord. Unfortunately, however, for case b, the maximum ratio achieved was only

**Fig. 4** Schematic of boundary conditions and loading conditions from simulation.**Fig. 3** Composite winglet predicted profiles.

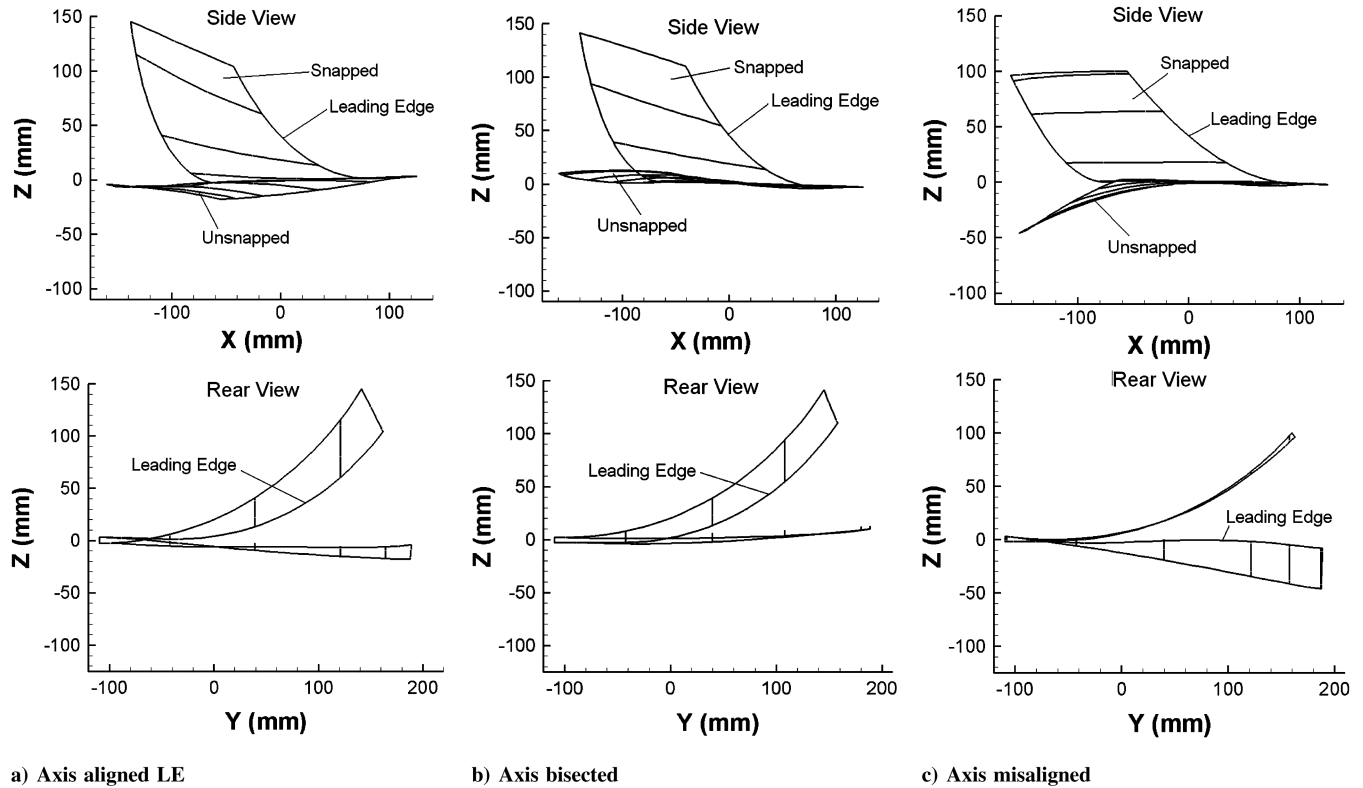


Fig. 5 Composite winglet predicted profiles; side and rear views.

$$\frac{h_{wl}}{c_{tip}} = \frac{0.142}{0.185} = 0.76$$

(see Fig. 5b).

Comparing results for the simulated reaction force vs displacement for all three configurations, Fig. 6 indicates very little change in the general behavior with changing fiber orientation. Four distinct regions of behavior are identifiable. Initially, with application of the external load, initial structural behavior resembles established linear-elastic structural characteristics (region i) before snap-through. Within this region, if the external load remains below a critical loading condition, the winglet behaves like a normal linear-elastic structure before nonlinear plastic deformation. However, with further increase in the loading condition, the composite enters region ii, in which the behavior becomes increasingly nonlinear, reaching a critical snap load shortly thereafter. At this position, the composite initiates the change from one stable state to the other (region iii). Within this region, the magnitude of the reaction force

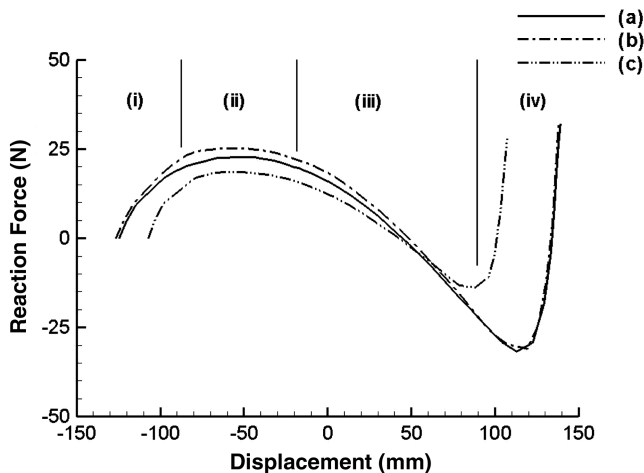


Fig. 6 Details of the predicted snap dynamics.

undergoes significant reduction and ultimately a change in sign. At this point, the composite now drives the change (negative structural stiffness), rather than reacting to oppose it. Upon reaching the final equilibrium condition at the end of region iii, further increase in applied load results in the return of classical linear-elastic structural behavior, as shown in region iv.

Although similar in form, results in Fig. 6 do show subtle differences with changes in fiber direction. For example, the reaction load required for snap-through was found to be 22.75, 25.20, and 18.62 N for cases a, b, and c, respectively, representing substantial decreases as the fiber direction is rotated both clockwise or anticlockwise from case b. Additionally, for cases a and b, the minimum reaction force was predicted at more than double that predicted for case c, which was substantial, given the small amount of relative fiber orientation imposed. Even so, if the maximum value of 25.2 N is taken as the required snap load during wind-tunnel testing, and with the wind tunnel running at near-maximum capability ($V = 40$ m/s), the extra increment in lift required by the winglet planform ($S_{wl} = 0.044$ m²) to initiate the snap was calculated at $\Delta C_{L_{wl}} \approx 0.6$. This value seemed reasonable and was considered to be well within the capabilities of the test rig proposed (Sec. III).

From the preceding analysis for the three winglet configurations investigated, the bistable winglet design with the fibers oriented parallel and perpendicular to a line bisecting the root and tip chords (case b) was chosen for manufacture and testing. Throughout the analysis of all of the designs, this particular layup orientation sequence was thought to best meet the criterion imposed on the different bistable geometrical configurations. Practically, this composite design was the only one that gave confidence to the authors that the efficient augmentation of lift in the unsnapped configuration was achievable, while still retaining some characteristics indicative of traditional winglet design in the snapped equilibrium condition. Although the predicted geometric displacements for the snapped case of this configuration were found to be less than ideal when compared with current winglet design methodologies, these inadequacies were tolerated to investigate the viability of the concept.

To manufacture the selected winglet configuration for the wind-tunnel testing phase, 8 rectangular lamina measuring 300 ×

200 mm of standard T300 carbon fiber with 914 Hexdite matrix prepreg were assembled and stacked in the sequence specified in Fig. 2. After assembly of the layup, the resulting winglet shape, paying particular attention to the direction of the fibers relative to the winglet planform shape, was cut out of the combined layup. The layup was then vacuum-sealed on a flat table and cured in an autoclave for 1 h at 170°C (heat-up rate between 2–5°C/min) and 7 bar pressure. Upon reaching this maximum temperature, these conditions were held constant for a period of 4 h, after which the autoclave automatically switched off, allowing the temperature field to dissipate naturally back down to standard room temperature. The resulting composite winglet (Fig. 7) was then removed, inspected, cleaned, and readied for wind-tunnel testing.

To establish confidence and validate the simulation procedure used with ABAQUS, both unsnapped and snapped winglet general geometric out-of-plane displacements were compared. In the unsnapped configuration (Fig. 7a), the degree of camber measured at the tip was found to be 4.8%, increasing to 7.4% at midspan. With the simulation predicting 3 and 6%, respectively, at these same locations for this unsnapped configuration, results seem to be somewhat underpredicted but are considered to be sufficient for the purposes of this work. Additionally, the local tip angle of attack for case b was predicted to be approximately zero, but as can be seen in Fig. 7a, a small degree of LE-up wing twist, with $\alpha_{tip} = 3.5$ deg, was measured. For the snapped condition (Fig. 7b), the deployed winglet height was also found to be different from that predicted. For this case, the maximum predicted winglet height was measured at 0.142 m (Figs. 3b and 5b). This was found to be marginally more than measurements taken from Fig. 7b at 0.124 m.

From the preceding discussion, generally speaking, it was considered that agreement between the predicted and experimental results was found to be reasonably good. However, these differences in initial and final winglet dimensions found between the simulated and experimental configurations could have arisen from many sources. Principally, such sources include the inherent discrepancies between the ability of the mathematical model to accurately predict the behavior of the experimental specimen, errors from imperfect

tooling, small levels of fiber misalignment during layup, and the assumption that the material properties of the laminas used perfectly matched the values used in the numerical computations. Additionally, subsequent to manufacture, it should also be noted that these composites remain susceptible to many outside influences that can change the geometric configuration and also the bistable properties. Primarily, the most significant influences come from exposure to significant temperature gradients and elevated levels of moisture in the air [23]. It is envisaged that combating these problems in practice will be difficult, particularly because both of these elements can be significant during aircraft flight. However, at this stage of the investigation, these factors were disregarded, as the main goal was to prove concept viability.

III. Experimental Setup and Apparatus

The experimental setup for the baseline swept-wing/winglet combination in the unsnapped and snapped configurations is shown in Fig. 8. The baseline swept wing for all testing used a Zagi 12 wing section, with a 30 deg leading-edge sweep, a wingspan of 0.6 m (baseline), zero washout, and root and tip chords of 0.326 m and 0.185 m, respectively. The wing was made of blue foam and reinforced with a bonded carbon and lacquered skin to maintain an aerodynamically robust surface finish. Attached at the quarter-chord point at the wing root, a purpose-built support bar (26 mm in diameter) was rigidly fixed to the internal structure of the wing via a machined insert, fasteners, and epoxy resin. A boundary-layer plate measuring 1.1 × 0.76 m and fixed at 0.05 m off the test-section side wall via adjustable bolts was used to minimize the effect of the wind-tunnel wall boundary layer contaminating the attachment line of the swept wing and resulting flowfield. To facilitate the installation of the swept wing, a 0.03-m-diam hole was cut out of this plate at midheight and 0.33 m from the leading edge to allow installation and mounting onto a six-axis force and moment balance.

The force and moment balance used to measure the response of the swept-wing test rig to aerodynamic loading was an AMTI MC3A-500. The maximum lift, drag, and side force capabilities of this cell

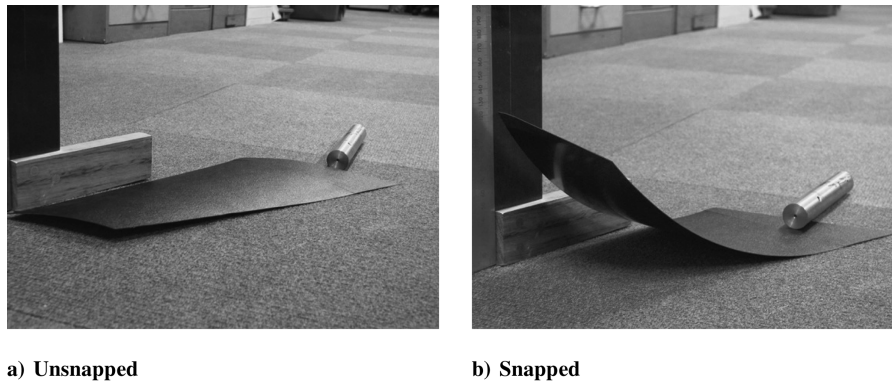


Fig. 7 Final actual winglet used in wind-tunnel testing.

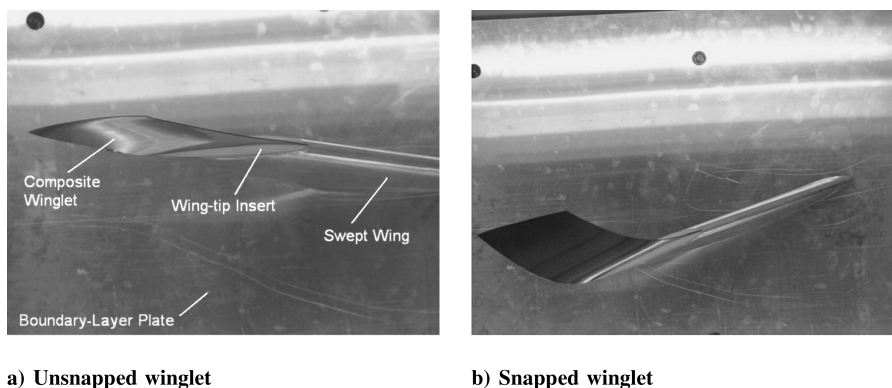


Fig. 8 Unsnapped and snapped winglet configurations.

were rated at ± 1 , ± 1 , and ± 2 kN, with pitching, rolling, and yawing moments specified at ± 56 , ± 56 , and ± 28 Nm, respectively. After calibration, maximum errors for all six components returned before the wind-tunnel testing was less than $\pm 2.5\%$. Assessment of the maximum observed nonlinearity as well as zero drift after a rigorous pretesting program were found to be better than $\pm 0.5\%$. All data obtained from the load cell was digitized through a 16-bit dSpace data acquisition system at 1000 Hz over a period of 60 s and was nondimensionalized with respect to the baseline (without winglet) swept-wing configuration.

The swept wing was installed at mid-test-section height inside a closed test section (height = 1.5 m and width = 2.1 m), closed-circuit wind tunnel with a maximum operating freestream velocity of 40 m/s ± 1 m/s. The freestream turbulence level at the model station was approximately 0.2%. Under test conditions, measurements of all six forces and moments were taken before increasing the wind speed, which allowed the compensation of the final test results for these initial conditions. To increase the aerodynamic loading on the winglet, the wind tunnel was brought up to speed manually and steadily by the operator until winglet snap was achieved. This process was repeated at several different angles of attack, ranging from 0–27.5 deg (position error ± 2 deg). For each of these angles of attack, the freestream velocity at the point of winglet snap was measured and recorded, giving a test Reynolds number range between 2.8×10^5 and 4.8×10^5 . No wind-tunnel blockage corrections or artificial transition-inducing mechanisms were used during the test program.

To protect the exposed portion of the swept-wing support bar between the wind-tunnel wall and the boundary-layer plate, a foam shroud, which encompassed the support bar completely, was fixed to the boundary-layer plate and extended all the way across to the wind-tunnel wall. This ensured that the flow could not induce any secondary loads on the swept-wing support bar. Upon exiting on the outside of the wind-tunnel wall, the support bar was attached to a purpose-built manual rotation stage, which allowed adjustment of the angle of attack of the swept wing. This manual rotation stage was also mounted directly onto the force and moment balance, which was connected to a support frame fixed to the outside test-section wall (Fig. 9).

At the tip of the baseline swept wing, an insert was designed and built to allow accurate and easy installation of the composite winglet. This insert was machined from nylon 6 and screwed into place using an array of small countersunk screws. Facilitated in the design of the insert was both a top and bottom half that used the mean camber line of the swept-wing profile as the dividing line. After fixing the winglet between these two sections, the whole assembly was mounted inside an excavated cavity engineered into the swept-wing tip.

IV. Results and Discussion

A. Preliminary Comments

Considering the results presented for all forces and moments before and after winglet snap shown in Fig. 10, both lift and drag force coefficients show trends with angle-of-attack change that are consistent with well-known wing aerodynamics [24]. These include the well-known C_D - α relationship, in which the drag is at a minimum for small values of angle of attack (thereafter increasing

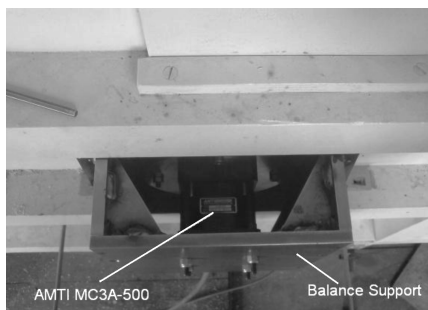


Fig. 9 Details of balance setup.

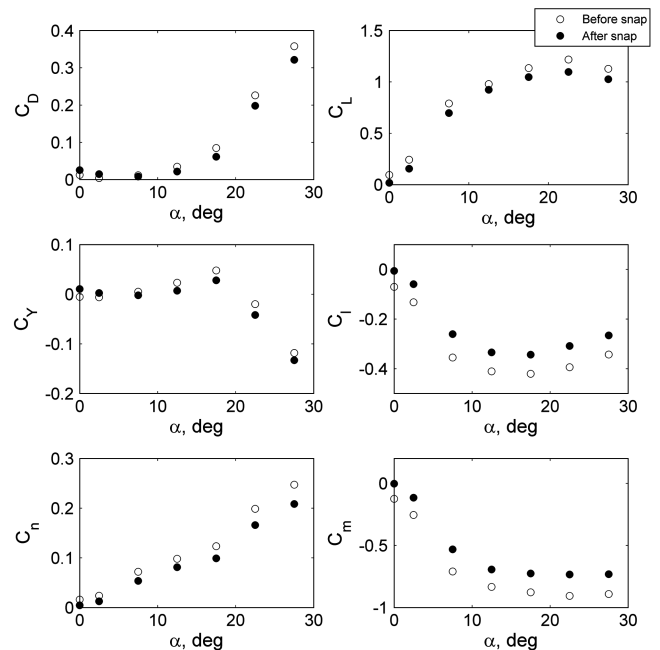


Fig. 10 Summary of aerodynamic forces and moments before and after snap.

nonlinearly), and an initial linear increase in lift, with increase in angle of attack. In this particular case of swept wing, this linear lift increase was found to persist up to approximately $\alpha = 12.5$ deg, diverging thereafter up to wing stall at $\alpha = 27.5$ deg. As would be expected due to the dependence on lift distribution, similar behavior was evident in results presented for rolling and pitching moment coefficients with comparable behavior on a similar model at a similar Reynolds number, discussed in [29]. For the remaining results of side force and yawing moment coefficients, both show trends significantly different from those already discussed. For the side force coefficient, the results tend to indicate a substantial and curious degree of inconsistency, first increasing up to $\alpha = 17.5$ deg, then decreasing thereafter up to the maximum angle of attack tested. At the two highest angles of attack tested, the side force coefficient is shown to reverse direction completely, suggesting unsteady stall conditions [30], possibly as a result of unsteady bursting phenomenon [31]. For the yawing moment coefficient, results show a similar trend to that already discussed for lift, pitching moment, and rolling moment coefficients for $\alpha \leq 12.5$ deg; however, after this angle of attack, the yawing moment coefficient is seen to increase markedly as the dependence on increasing wing drag levels becomes more and more significant.

For the unsteady rms force and moment coefficients presented in Fig. 11, all show a degree of inconsistency between trends in results before and after winglet snap, with some results at some angles of attack showing larger magnitudes of unsteadiness before snap than after, and showing the reverse at other angles of attack. Generally, however, evident in all the results presented is the general trend of increasing unsteadiness (almost linearly) with increasing angle of attack as a precursor to wing stall [32]. For $\alpha \leq 12.5$ deg, most results presented show unsteady levels invariant between the before- and after-snap conditions, indicating a degree of similitude between these two conditions. However, this behavior was not found to persist above these levels of angle of attack, as both increasing differential magnitudes (between before and after snap) as well as overall unsteady magnitudes were found to increase.

When comparing the magnitudes of the forces and moments coefficients in Figs. 10 and 11, the degree of unsteadiness as a percentage of the mean result is significant and constitutes a substantial portion of the overall aerodynamic behavior. At low angles of attack, for instance ($\alpha \leq 17.5$ deg), the rms coefficient superimposed on the average magnitude was found to constitute (particularly for the drag, side force, and yawing moment

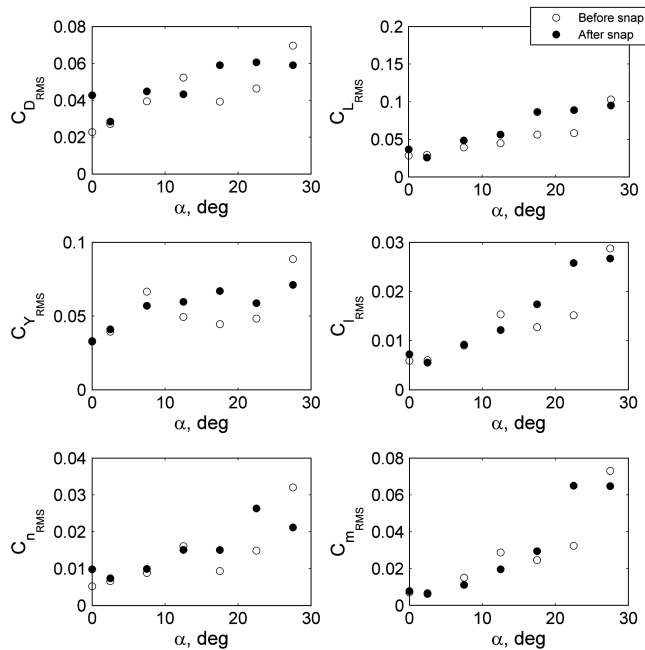


Fig. 11 RMS aerodynamic forces and moments before and after snap.

coefficients), a component that was several times greater than the mean magnitude. This result clearly outlines the unsteady nature of the flowfield/swept-wing combination at this Reynolds number. At higher angles of attack ($\alpha \geq 17.5$ deg), whereas unsteadiness magnitude increased further, this component as a percentage of the overall magnitude was found to decrease to levels that were approximately 50% of the mean magnitude (Fig. 10).

B. Effect of Winglet Snap on Aerodynamic Performance

In Fig. 10, for all angles of attack tested, most aerodynamic force and moment results show a measurable decrease in mean magnitude after winglet snap. From the results of lift force, the extra lift augmentation generated by the composite winglet was found to range between $0.055 \leq \Delta C_L \leq 0.12$ within the angle-of-attack range presented ($\Delta C_L = 0.12$ at $\alpha = 22.5$ deg). Unfortunately, at low angles of attack of $\alpha \leq 7.5$ deg with the change in lift coefficient being between $0.08 \leq \Delta C_L \leq 0.1$, the performance of the bistable winglet did not compare well with existing advanced high-lift systems installed on swept-wing configurations ($\Delta C_L \approx 0.6$ for split flaps and $\Delta C_L \approx 1.5$ for double-slotted flaps at low speeds and $\alpha = 0$ deg) [24,26,33,34]. However, when considering the results for the drag coefficient shown in Fig. 10, at low angles of attack ($\alpha \leq 2.5$ deg), the mean drag coefficient measured after snap is marginally more ($\Delta C_D \approx 0.01$) than that indicated before snap. Although the results clearly suggest that the winglet is outperformed by more traditional high-lift systems in the production of extra lift (not taking into account any relative weight savings from using the winglet concept), for small angles of attack ($\alpha \leq 2.5$ deg), results also suggest that there is a small but measurable decrease in drag coefficient (compared with the snapped configuration) before snap, most probably resulting from a combination of both the increase in effective aspect ratio before snap (decreasing induced drag for the same C_L before and after snap) and/or an increase in winglet profile drag after snap. Unfortunately, this trend did not persist for $\alpha \geq 7.5$ deg, with this difference in drag coefficient before and after winglet snap decreasing to approximately zero ($\alpha = 7.5$ deg) and thereafter increasing almost linearly up to a maximum of $\Delta C_D \approx 0.028$ at $\alpha = 27.5$ deg.

Comparing the results for the aerodynamic moment coefficients presented in Fig. 10 before and after snap, similar trends to that already described for the change in lift coefficient were evident for both ΔC_l and ΔC_m , with almost a consistent change found for all angles of attack tested. This result was expected due to the inherent

dependency of these two moments on the lift distribution. For these rolling and pitching moment coefficients, the incremental difference in winglet performance between the unsnapped and snapped configurations was measured in the range of $-0.076 \leq \Delta C_l \leq -0.094$ and $-0.140 \leq \Delta C_m \leq -0.178$, respectively. Typical increments in pitching moment coefficient from the deployment of more traditional high-lift systems (on swept wings) can range from $\Delta C_m = -0.05$ for split flaps [34] to $\Delta C_m = -0.29$ for double-slotted flaps [34]. Using these results for comparison, it therefore seems that the corrective measures required by the aircraft control system during winglet deployment would be comparable with the corrective measures required by the more advanced and complex high-lift systems in use today. This result, even at the moderate levels of lift augmentation already discussed, is an unfortunate consequence of the inherent increased moment arm when the winglet is installed at the swept-wing tip.

Another interesting aspect of the winglet concept to consider was the magnitude of the freestream velocity measured at winglet snap with increase in angle of attack (Table 2). At $\alpha = 0$ deg, the freestream velocity to snap the winglet was measured at 27 m/s. Under these conditions, the resultant aerodynamic force acts almost coincident with a line perpendicular to the primary snapping axis of the winglet. As the angle of attack increased, the dynamic pressure required for winglet snap was shown to decrease rapidly, reaching a minimum of 16 m/s at $\alpha = 7.5$ deg. At this angle of attack, the rapidly increasing resultant aerodynamic force, together with the line of action of this force remaining largely perpendicular to the primary snap axis of the winglet, more easily generates the snapping moment required at a lower dynamic pressure. At higher angles of attack, however, the magnitude of the freestream velocity was found to remain constant within the region of 16–17 m/s for winglet snap, with the differential lift force generated by the winglet also showing consistency ($\Delta C_L \approx 0.1$ in Fig. 10). This suggests conditions in which flow separation may have already occurred from the sharp leading edge of the winglet [26]. Ultimately, a constant value for the lift generated by the winglet would suggest that the snap velocity would again increase from this minimum; however, from $\alpha = 12.5$ to 27.5 deg, the drag force acting on the winglet increases rapidly (indicative from the results in Fig. 10), compensating somewhat for the reduced contribution from $\Delta C_{L_{wl}}$ to snap the winglet.

C. Winglet-Snap Dynamics

To quantify the severity of this snap-through, Fig. 12 gives an example of the dynamic responses of all six aerodynamic force and moment coefficients of the swept-wing/composite winglet combination as dynamic pressure increased. At first inspection, all results show substantial degrees of increasing unsteadiness with increase in dynamic pressure. Figure 11 quantifies this degree of unsteadiness for the conditions just before and after snap. As can be seen from this figure, and when comparisons are made with Fig. 10, particularly for the drag and side force coefficients, the degree of unsteadiness as a proportion of mean magnitude made the determination of mean values difficult and, in some cases (particularly at low angles of attack), unreliable. However, some interesting and useful insight into the physics and mechanics of the winglet-snap process at these levels of angle of attack could still be gauged. For instance, in Fig. 12, for all results, after the initial linear increase in aerodynamic loading (≈ 10 – 40 s) after wind-on conditions, the extent of the maximum and minimum dynamic loads applied to the test rig and the speed of the transition between the two stable states were both found to be particularly severe. In most cases, force and moment coefficient magnitudes at snap were more than several hundred percent greater than the presnap or postsnap

Table 2 Summary of winglet-snap freestream velocity with angle of attack

Angle of attack, deg	0	2.5	7.5	12.5	17.5	22.5	27.5
Snap velocity, m/s	27	23	16	16	17	17	16.5

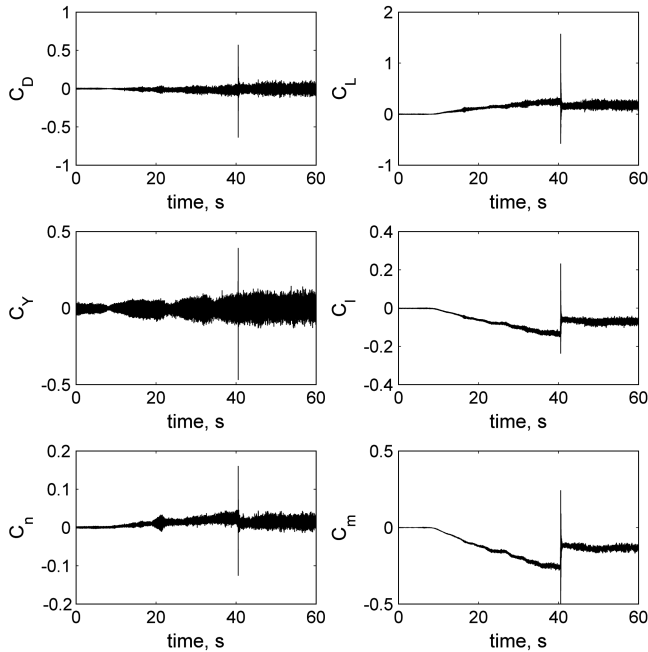


Fig. 12 Example of the response of the composite winglet and swept-wing combination: $\alpha = 2.5$ deg.

magnitudes. Figure 13 quantifies these results. Additionally, in Fig. 13, there clearly exists an almost consistent offset between the maximum and minimum amplitudes at snap for the drag and side force coefficients as well as the yawing moment coefficient. However, results for the lift coefficient as well as the rolling and pitching moment coefficients indicate some variation in this offset, particularly at lower angles of attack, with values for the maximum and minimum dynamic loads (when compared with the mean result) showing asymmetry toward the maximum (i.e. $C_{L_{\max}} = 1.575$, $C_{L_{\min}} = -0.578$, and $C_{L_{\text{bs}}} = 0.243$ at $\alpha = 2.5$ deg).

Considering the real-time responses shown in Fig. 12 more closely, a more detailed view of the winglet-snap dynamics for the lift force coefficient and all three moment coefficients is presented in Fig. 14. From these subfigures, all aerodynamic parameters

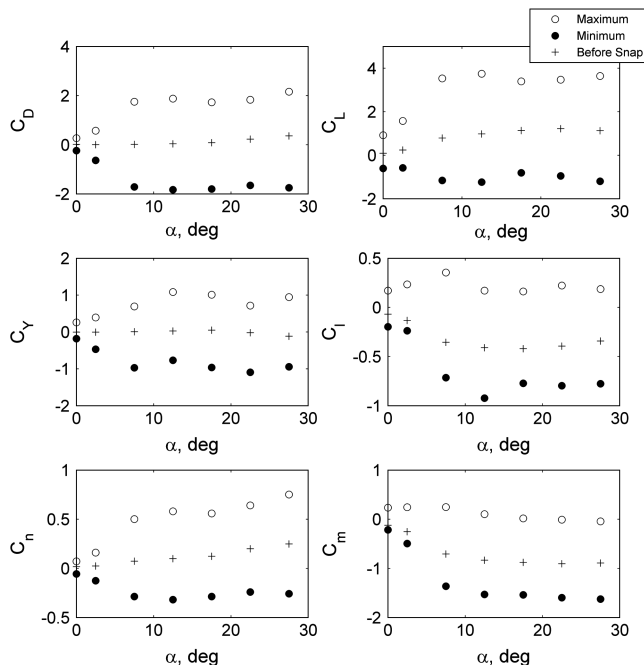


Fig. 13 Maximum and minimum aerodynamic forces and moments during snap-through.

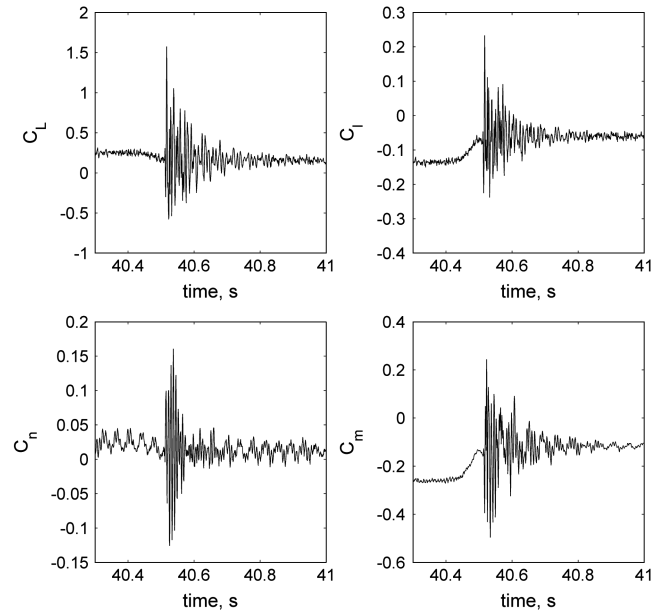


Fig. 14 Detailed response of lift force and all moments to composite winglet snap: $\alpha = 2.5$ deg.

presented are shown to exhibit a reduction in magnitude to levels that are consistent with the postsnap magnitude just before winglet snap. For the case presented in Fig. 14, this reduction began at approximately 40.45 s and lasted 0.06 s before the full dynamic effects of the winglet snap were initiated (40.51 s). At this instant in time, the large-amplitude dynamic loads, discussed earlier, are initiated as the winglet moves through the snap process. Typically, the maximum and minimum loading conditions are established for 0.01 s each, representing increases and decreases of up to several hundred percent, compared with the mean values during this time frame. After this time period in which the maximum and minimum occur, the dynamic loads undergo characteristic damped vibration over a period of 0.2–0.4 s before the reestablishment of the postsnap steady-state value. The entire dynamic snap process, from initiation to the reestablishment of steady-state conditions, was found to occur over a time period of 0.45–0.5 s.

As mentioned in Sec. IV.B, although being within the typical correction range for modern elevator systems during deployment, it is conceivable that, due to this speed of snap transition, the demands on the frequency response of modern elevator control systems may be unrealistic. If this is indeed the case, the integration of the bistable winglets onto an aircraft wing in this pure form would clearly represent an unacceptable degree of passenger discomfort as well as safe and achievable control. For the rolling and yawing moments, it would be expected that these effects, if actuated simultaneously, would be less problematic, as the effects of a pair of winglets would cancel each other out. Having to correct a significant and sudden nose pitch-up moment just after takeoff, after winglet snap, poses a much more serious problem. Under these conditions, in which the possibility of aircraft stall increases, it would be imperative, if adopted, to develop system(s) that could slow, synchronize, and/or control the snap process [35] as well as ensure stability after snap-through [36].

V. Conclusions

A novel concept using a bistable winglet to augment lift generation on a generic swept wing transitioning from lower to higher subsonic flow speeds is presented in this paper. The composite winglet, which was specifically designed using an unsymmetric layup sequence, was found to produce a measurable degree of lift augmentation at the first stable state with the span fully extended and the chordwise profile cambered, when compared with the final stable state, in which the aerodynamic shape was more indicative of traditional winglet design. However, results also showed that during the snap-through

process, significant dynamic loads were produced and transmitted throughout the entire wing structure, suggesting that additional attenuation and/or control methodologies will be required to ensure practical application to modern aircraft operations.

Acknowledgment

This work has been supported by a Marie-Curie excellence research grant MEXT-CT-2003-002690 funded by the European Commission.

References

- [1] Jha, A. K., and Kudvasmart, J. N., "Morphing Aircraft Concepts, Classifications, and Challenges," *Structures and Materials 2004: Industrial and Commercial Applications of Smart Structures Technologies*, Proceedings of SPIE, Vol. 5388, Society of Photo-Optical Instrumentation Engineers, Bellingham, WA, Mar. 2004, pp. 213–224.
- [2] Sanders, B., Eastep, F. E., and Forster, E., "Aerodynamic and Aeroelastic Characteristics of Wings with Conformal Control Surfaces for Morphing Aircraft," *Journal of Aircraft*, Vol. 40, No. 1, 2003, pp. 94–99.
doi:10.2514/2.3062
- [3] Hall, J. M., "Executive Summary AFTI/F-111 Mission Adaptive Wing," Wright Research and Development Center, TR-89-2083, Wright-Patterson AFB, OH, 1989.
- [4] Knot, N. S., Zweber, J. V., Velej, D. E., Oz, H., and Eastep, F. E., "Flexible Composite Wing with Internal Actuation for Roll Manoeuvre," *Journal of Aircraft*, Vol. 39, No. 4, 2002, pp. 521–527.
doi:10.2514/2.2971
- [5] Johnston, C. O., Mason, W. H., Han, C., and Inman, D. J., "Actuator-Work Concepts Applied to Unconventional Aerodynamic Control Devices," *Journal of Aircraft*, Vol. 44, No. 5, 2007, pp. 1459–1468.
doi:10.2514/1.26423
- [6] Stanewsky, E., "Aerodynamic Benefits of Adaptive Wing Technology," *Aerospace Science and Technology*, Vol. 4, No. 7, 2000, pp. 439–452.
doi:10.1016/S1270-9638(00)01069-5
- [7] Stanewsky, E., "Adaptive Wing and Flow Control Technology," *Progress in Aerospace Sciences*, Vol. 37, No. 7, 2001, pp. 583–667.
doi:10.1016/S0376-0421(01)00017-3
- [8] Schultz, M. R., and Hyer, M. W., "A Morphing Concept Based on Unsymmetric Composite Laminates and Piezoceramic MFC Actuators," 45th AIAA/ASME/ASCE/AHS/ASC Structures, Structural Dynamics and Materials Conference, Palm Springs, CA, AIAA Paper 2004-1806, Apr. 2004.
- [9] Dano, M. L., and Hyer, M. W., "SMA-induced Snap-Through of Unsymmetric Fiber-Reinforced Composite Laminates," *International Journal of Solids and Structures*, Vol. 40, No. 22, Nov. 2003, pp. 5949–5972.
doi:10.1016/S0020-7683(03)00374-3
- [10] Whitmer, C. E., and Kelkar, A. G., "Robust Control of a Morphing Airfoil Structure," *American Control Conference*, Inst. of Electrical and Electronics Engineers, Piscataway, NJ, June 2005, pp. 2863–2868.
- [11] Campanile, L. F., "Lightweight Shape-Adaptable Airfoils: A New Challenge for an Old Dream," *Adaptive Structures: Engineering Applications*, Wiley, Chichester, England, U.K., 2007.
- [12] Lu, K. J., and Kota, S., "Design of Compliant Mechanisms for Morphing Structural Shapes," *Journal of Intelligent Material Systems and Structures*, Vol. 14, No. 6, 2003, pp. 379–391.
doi:10.1177/1045389X03035563
- [13] Crouch, T. D., *Wings: A History of Aviation from Kites to the Space Age*, Norton, New York, 2004.
- [14] Williams, A. L., "A New and Less Complex Alternative to the Handley Page Slat," *Journal of Aircraft*, Vol. 23, No. 3, 1986, pp. 200–206.
doi:10.2514/3.45289
- [15] Balaji, R., Bramkamp, F., Hesse, M., and Ballmann, J., "Effect of Flap and Slat Riggings on 2-D High-Lift Aerodynamics," *Journal of Aircraft*, Vol. 43, No. 5, 2006, pp. 1259–1271.
doi:10.2514/1.19391
- [16] Heragu, S. S., "Prediction of Turbulent Flow Behavior over a Slotted Flap," *Journal of Aircraft*, Vol. 29, No. 1, 1992, pp. 52–62.
doi:10.2514/3.46124
- [17] Petz, R., and Nitsche, W., "Active Separation Control on the Flap of a Two-Dimensional Generic High-Lift Configuration," *Journal of Aircraft*, Vol. 44, No. 3, 2007, pp. 865–874.
doi:10.2514/1.25425
- [18] Englar, R. J., Smith, M. J., Kelley, S. M., and Rover, R. C., "Application of Circulation Control to Advanced Subsonic Transport Aircraft, Part 2: Transport Application," *Journal of Aircraft*, Vol. 31, No. 5, 1994, pp. 1169–1177.
doi:10.2514/3.46627
- [19] Torenbeek, E., *Synthesis of Subsonic Aeroplane Design*, Kluwer Academic, Dordrecht, The Netherlands, 1982.
- [20] de Mattos, B. S., Macedo, A. P., and da Silva Filho, D. H., "Considerations about Winglet Design," 21st Applied Aerodynamics Conference, Orlando, FL, AIAA Paper 2003-3502, 23–26 June 2003.
- [21] Schioler, T., and Pellegrino, S., "Multi-Configuration Space Frames," 45th AIAA/ASME/ASCE/AHS/ASC Structures, Structural Dynamics and Materials Conference, Palm Springs, CA, AIAA Paper 2004-1529, Apr. 2004.
- [22] Jun, W. J., and Hong, C. S., "Effect of Residual Shear Strain on the Cured Shape of Unsymmetric Cross-Ply Thin Laminates," *Composites Science and Technology*, Vol. 38, No. 1, 1990, pp. 55–67.
doi:10.1016/0266-3538(90)90071-C
- [23] Mattioni, F., Weaver, P. M., Potter, K. D., and Friswell, M. I., "Analysis of Thermally Induced Multistable Composites," *International Journal of Solids and Structures*, Vol. 45, No. 2, Jan. 2008, Paper 657675.
- [24] Stinton, D., *The Design of the Airplane*, Blackwell Science, London, 2001.
- [25] Raymer, D. P., *Aircraft Design: A Conceptual Approach*, 4th ed., AIAA Education Series, New York, 2006.
- [26] Abbott, I. H., and von Doenhoff, A. E., *Theory of Wing Sections: Including a Summary of Airfoil Data*, Dover, New York, 1959.
- [27] Whitcomb, R. T., "A Design Approach and Selected Wind-Tunnel Results at High Subsonic Speeds for Wing-Tip Mounted Winglets," NASA TN D-8260, 1976.
- [28] *Aerodynamic Principles of Winglets*, ESDU International, London, 1998.
- [29] Gerontakos, P., and Lee, T., "Near-Field Tip Vortex behind a Swept Wing Model," *Experiments in Fluids*, Vol. 40, No. 1, 2006, pp. 141–155.
doi:10.1007/s00348-005-0056-y
- [30] Orlik-Ruckemann, K., "Aerodynamic Aspects of Aircraft Dynamics at High Angles of Attack," *Journal of Aircraft*, Vol. 20, No. 9, 1983, pp. 737–752.
doi:10.2514/3.44938
- [31] Johnson, J. L., Grafton, S. B., and Yip, L. P., "Exploratory Investigation of the Effects of Vortex Bursting on the High-Angle-of-Attack Lateral-Directional Stability Characteristics of Highly-Swept Wings," 11th Aerodynamic Testing Conference, Colorado Springs, CO, AIAA Paper 80-0463, Mar. 1980.
- [32] Taylor, G. S., and Gursul, I., "Buffeting Flows over a Low-Sweep Delta Wing," *AIAA Journal*, Vol. 42, No. 9, 2004, pp. 1737–1745.
doi:10.2514/1.5391
- [33] Gratzler, L. B., "Analysis of Transport Applications for High-lift Schemes," *Assessment of Lift Augmentation Devices*, AGARD Rept. LS-43-71, Neuilly-sur-Seine, France, 1971.
- [34] *Information on the Use of Data Items on High Lift Devices*, ESDU International, London, 1997.
- [35] Schultz, M. R., Hyer, M. W., Williams, R. B., Wilkie, W. K., and Inman, D. J., "Snap-Through of Unsymmetric Laminates Using Piezocomposite Actuators," *Composites Science and Technology*, Vol. 66, No. 14, Nov. 2006, pp. 2442–2448.
doi:10.1016/j.compscitech.2006.01.027
- [36] Canfield, R. A., Morgenstern, S. D., and Kunz, D. L., "Alleviation of Buffet-Induced Vibration Using Piezoelectric Actuators," *Computers and Structures*, Vol. 86, Nos. 3–5, Feb. 2008, pp. 281–291.
doi:10.1016/j.compstruc.2007.02.027